ORIGINAL ARTICLE | **Open Access**

Defect-related blue emission from ultra-fine $Zn_{1-x}Cd_xS$ quantum dots synthesized by simple beaker chemistry

Jeotikanta Mohapatra

Abstract

It has been possible to incorporate cadmium ions in ZnS quantum dots (QDs). It is studied how the substitution of Cd^{2+} ions by zinc ions affects the structural, morphological, and optical properties of ZnS QDs. $Zn_{1-x}Cd_xS$ QDs are prepared by a simple beaker chemistry approach and characterized by X-ray diffraction (XRD), high-resolution transmission electron microscopy, and UV-visible and photoluminescence (PL) spectroscopies. XRD studies confirmed that all the prepared samples are in zinc-blende phase. With the increase of cadmium content, the diffraction peaks shifted towards lower diffraction angles and the lattice constant increased linearly. Optical studies revealed that the strong absorption edge also shifted towards the higher wavelength region with the increase of Cd content. Hence, the optical bandgap of the QDs decreases with the increase of Cd content. Due to the quantum confinement of the carriers in the QDs, the bandgap energy is higher than that of the corresponding bulk material. The PL spectrum of the undoped ZnS QDs contains five peaks (centered at 365, 400, 420, 450, and 470 nm) which are attributed to the recombination of the defect states of ZnS.

Keywords: Quantum dots, Beaker chemistry, Optical properties

Background

Nanocrystalline solid solutions are very attractive materials because of their potential to control the optical properties by varying the solution composition as well as the particle size. In the case of ZnS, the bandgap varies in the range of 3.7 to 5.5 eV depending upon the particle size in the nanoregime [1,2]. However, by incorporating Cd^{2+} ions into ZnS nanocrystals, $Zn_{1-x}Cd_xS$ solid-solution semiconductors have been made and their energy bandgap was found to vary from 5.5 to 2.5 eV at room temperature [2-4]. As a consequence, the absorption edge shifts towards lower energy with the increase of Cd content. The quantization of bandgap in ZnS shows blue-green emission arising from defect states [2,5]. However, the emission spectra of cubic cadmium-doped ZnS (ZnS:Cd) quantum dots (QDs) were reported to cover the entire visible spectrum by varying the Cd^{+2}/Zn^{+2} ratios [6,7].

Herein, a simple beaker chemistry approach is demonstrated to synthesize ultra-fine $Zn_{1-x}Cd_xS$ QDs at room temperature. Transmission electron microscopy (TEM) results confirm that the incorporation of Cd ions (x from 0 to 0.5) in ZnS QDs leads to an increase in the particle size from 4 to 7 nm. A similar trend for the increases of particle size with Cd content is also observed from X-ray diffraction (XRD) and UV-visible measurements. Photoluminescence spectra show an increase of the strain on the QD surface with the increase of Cd content, and it leads to increases in the intensity of the 470-nm peak.

Methods

$Zn_{1-x}Cd_xS$ ($0 \leq x \leq 0.5$) QDs were prepared at room temperature without using any capping agent or surfactant via beaker chemistry. The preparation of $Zn_{1-x}Cd_xS$ nanocrystallite powders was carried out in two steps. In the first step, two different solutions, solution I and solution II, were prepared separately. Solution I was prepared by dissolving an appropriate amount of cadmium acetate dihydrate and zinc acetate dihydrate such that the total amount of these two salts was 10 mmol in 30

Correspondence: pinuphy@gmail.com
Centre for Research in Nanotechnology and Science (CRNTS), Indian Institute of Technology Bombay, Powai, Mumbai 40076, India

ml methanol. In solution II, a saturated solution of sodium sulfide monohydrate was prepared by dissolving Na_2S in 20 ml methanol. In the second step, solution I was first vigorously stirred using a magnetic stirrer for 30 min, and then solution II was added to solution I dropwise and stopped when the pH of the solution becomes 8. The whole reaction was carried out at room temperature. The mixed thick solution was stirred for 1 h to complete the chemical reaction. The precipitate was separated by centrifugation at 8,000 rpm for 6 min and washed several times with methanol to remove sodium ions. Then the washed precipitate was dried to collect the finally prepared $Zn_{1-x}Cd_xS$ QDs. The Cd composition x was controlled as 0, 0.01, 0.04, 0.1, 0.2, 0.3, and 0.5. A brief pictorial detail of the synthesis procedure is given in Figure 1.
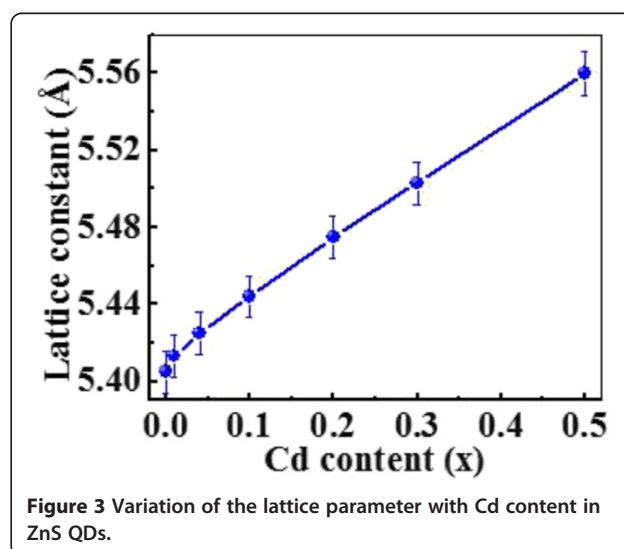
The X-ray diffraction pattern confirmed the formation of $Zn_{1-x}Cd_xS$ phase. The X-ray diffraction pattern was recorded using an X-ray diffractometer (PANalytical, Almelo, The Netherlands) using Cu Kα radiation of wavelength λ = 0.15406 nm. The transmission electron microscope (JEOL JEM 2100F, Akishima-shi, Japan) study confirmed the formation of $Zn_{1-x}Cd_xS$ QDs. The optical transmission/absorption spectra of $Zn_{1-x}Cd_xS$ QDs were recorded using a UV–Vis spectrophotometer (U-3010, Hitachi, Chiyoda-ku, Japan). For optical measurement, the sample powders were dispersed in methanol. The photoluminescence (PL) spectrum of $Zn_{1-x}Cd_xS$ QDs dispersed in methanol was measured using a spectrofluorimeter (F-2500 FL Spectrophotometer, Hitachi).
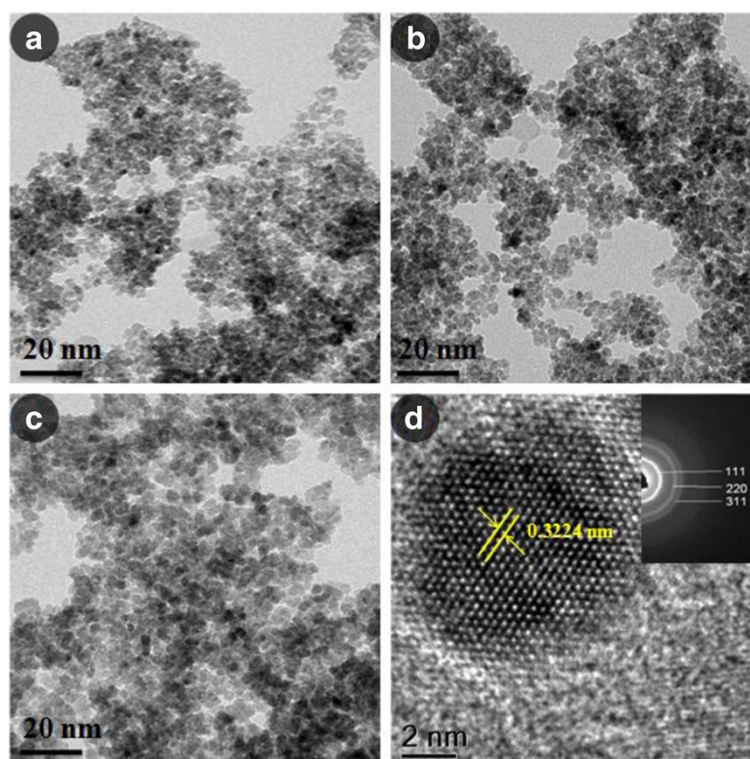
Results and discussion

Figure 2 shows the XRD patterns of the $Zn_{1-x}Cd_xS$ QDs for different values of x (mole percentage of cadmium),

Figure 2 XRD patterns of the $Zn_{1-x}Cd_xS$ QDs produced with different mole fractions (*x*) of Cd.
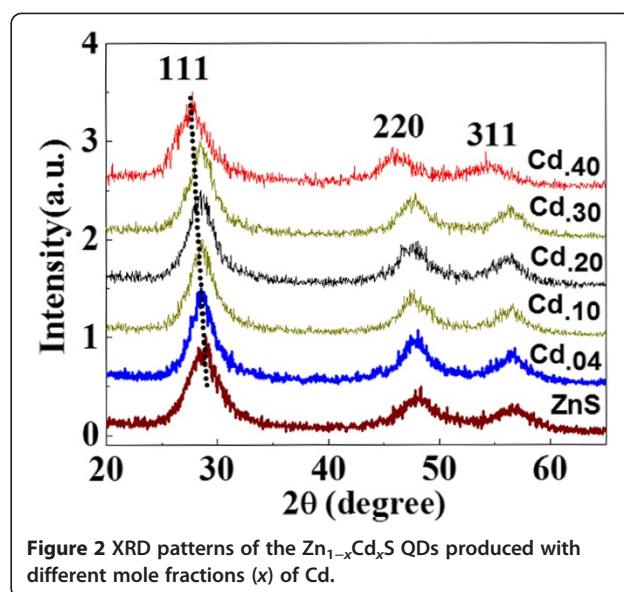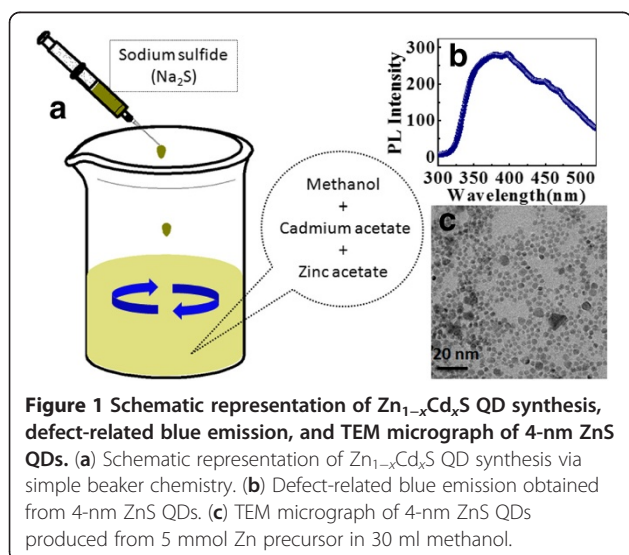
which indicates that all samples are of zinc-blende (cubic) structure (JCPDS card no. 5–566) [8]. The characteristic XRD patterns of $Zn_{1-x}Cd_xS$ QDs exhibit three prominent peaks which correspond to (111), (220), and (311) planes of the cubic phase of ZnS with the lattice constant a = 5.4 Å (JCPDS card no. 80-0020) [9]. The diffraction peak positions also gradually shifted towards lower diffraction angles as the Cd concentration increased from 0 to 0.5, which indicates that the crystals obtained are not a mixture of pure ZnS and CdS rather a $Zn_{1-x}Cd_xS$ solid solution [8,10]. The variation of lattice parameter a estimated from XRD data with x is shown in Figure 3, which shows a linear increase of the lattice constant from 5.405 to 5.560 Å with the increase of Cd content x from 0 to 0.5. A similar trend has also been

Figure 1 Schematic representation of $Zn_{1-x}Cd_xS$ QD synthesis, defect-related blue emission, and TEM micrograph of 4-nm ZnS QDs. (**a**) Schematic representation of $Zn_{1-x}Cd_xS$ QD synthesis via simple beaker chemistry. (**b**) Defect-related blue emission obtained from 4-nm ZnS QDs. (**c**) TEM micrograph of 4-nm ZnS QDs produced from 5 mmol Zn precursor in 30 ml methanol.

Figure 3 Variation of the lattice parameter with Cd content in ZnS QDs.

Figure 4 Representative TEM images of Zn$_{1-x}$Cd$_x$S QDs and HRTEM image of a single QD. TEM images of Zn$_{1-x}$Cd$_x$S QDs with Cd content of (**a**) x = 0.04, (**b**) x = 0.1, and (**c**) x = 0.5. (**d**) HRTEM image of a single QD produced with Cd content x = 0.5, and the inset shows the SAED pattern.

reported earlier [10,11]. This linear increase in lattice parameter a with the increase of Cd content confirms the formation of a homogenous solid solution of Zn$_{1-x}$Cd$_x$S nanostructure. The small difference in the bond length of ZnS and CdS and the very close electronegativity value of Cd and Zn allow the formation of solid-solution materials.

Figure 4a,b,c shows the TEM images of Zn$_{1-x}$Cd$_x$S QDs having Cd concentrations of 0.04, 0.1, and 0.5, respectively. The average particle sizes estimated are 4.5 ± 0.5 nm (σ = ±10%) for the x = 0.01 sample, 5 ± 0.5 nm (σ = ±10%) for the x = 0.1 sample, and 7 ± 1 nm (σ = ±15%) for the x = 0.5 sample, and this is consistent with the particle sizes estimated from XRD spectra (by using the Scherrer formula; see Table 1). Figure 4d shows the high-resolution transmission electron microscopy (HRTEM) image of QDs produced with Cd concentration x = 0.5 which confirms the crystallinity of the as-synthesized QDs. The inset of Figure 4d represents the selected-area electron diffraction (SAED) pattern. As expected, the SAED pattern shows a set of rings instead of spots due to the random orientation of the crystallites, corresponding to reflections from three crystal planes: (111), (220), and (311). This confirms the formation of a cubic phase of ZnS. The interplanar spacings (d_{hkl}) calculated from XRD and SAED are summarized in Table 2 for Zn$_{1-x}$Cd$_x$S (with x = 0.04, 0.1, 0.5). Figure 5a,b shows the energy-dispersive X-ray (EDAX) spectra of the Zn$_{1-x}$Cd$_x$S QDs with Cd atomic fraction x = 0.04 and 0.1, respectively, which confirms the stoichiometric composition of the prepared samples.

Figure 6 shows the UV-visible absorption spectra of the Zn$_{1-x}$Cd$_x$S QDs. In pristine ZnS QDs, the excitonic peak appears at a wavelength around 312 nm. This peak

Table 1 Comparison of bandgap energy and size of Zn$_{1-x}$Cd$_x$S QDs produced with different Cd concentrations

Cd concentration (%)	Optical bandgap energy of nanocrystal E_g (eV)	Particle size from XRD (nm)	Particle size estimated from UV-vis data (nm)
1	4.1	4.8	4.6
4	4.0	5.1	5.0
10	3.9	5.4	5.1
20	3.8	5.9	5.5
30	3.7	6.4	5.9
50	3.4	6.8	6.3

Table 2 Comparison of interplanar spacing (d_{111}) obtained from XRD and SAED for $Zn_{1-x}Cd_xS$ QDs with x = 0.04, 0.1, and 0.5

Sample name	d_{111} from XRD (nm)	d_{111} from SAED (nm)	Particle size from TEM (nm)
$Zn_{.96}Cd_{.04}S$	0.312	0.312	5 ± 0.5
$Zn_{.90}Cd_{.10}S$	0.313	0.314	6 ± 0.5
$Zn_{.50}Cd_{.50}S$	0.3254	0.323	7 ± 1

position reflects the excitonic binding energy of QDs. Moreover, with increases of Cd content in ZnS, the excitonic peak which is a characteristic of QDs gradually shifts towards a higher wavelength. The red shift is attributed to quantum confinement effect as well as the increase of Cd concentration (as the particle size increases with respect to the increases of Cd content) [12].

The fundamental absorption, which corresponds to the transition from the valence band to the conduction band, can be used to determine the optical bandgap of the material. From the transmission data, the absorption coefficient (α) at different wavelengths λ is calculated using Beer-Lambert's relation (reflection/scattering is negligible due to the small size of the particle), given by

$$\alpha = \frac{1}{d}\ln\left(\frac{1}{T}\right) \qquad (1)$$

The relation between α and the incident photon energy ($h\nu$) can be written as [12]

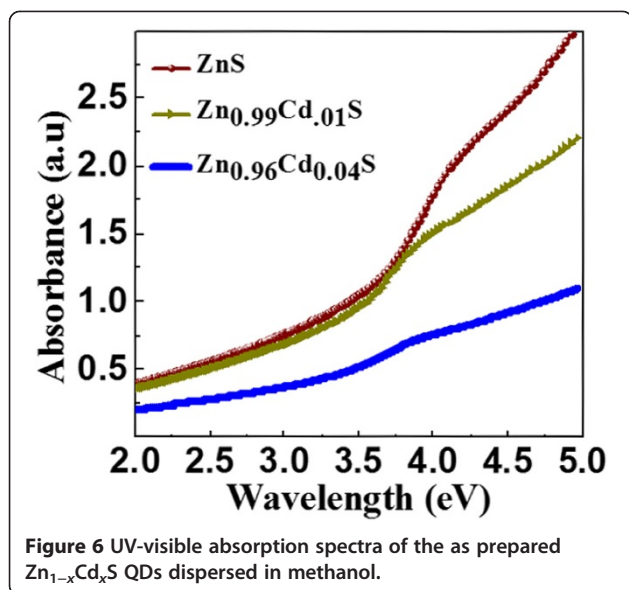$$\alpha = \left(\frac{A}{h\nu}\right)(h\nu - Eg)^m \qquad (2)$$

where A is a constant, E_g is the bandgap of the material, and the exponent m depends on the type of transition. The exponent m has the values 1/2, 2, 3/2, and 3 corresponding to the allowed direct, allowed indirect, forbidden direct, and forbidden indirect transitions, respectively. The bandgap can be estimated from the plot of $(\alpha h\nu)^{1/m}$ versus $h\nu$, where m indicates the nature of optical transition in the material. For bulk semiconductors with direct transition, $m = 0.5$. In a nanocrystalline material, the nature of optical transition can be different from that in the bulk as mentioned earlier. Therefore, to avoid any preassumption, the values of m for $Zn_{0.9}Cd_{0.1}S$ QDs were determined as discussed below. Now Equation 2 can be written as follows:

$$\frac{d\ln(\alpha h\nu)}{d(h\nu)} = \left(\frac{m}{h\nu - E_g}\right) \qquad (3)$$

So, there should be a discontinuity in the $d(\ln(\alpha h\nu))/d(h\nu)$ versus $h\nu$ plot at the bandgap energy. A representative plot of $d(\ln(\alpha h\nu))/d(h\nu)$ versus $h\nu$ is presented in Figure 7a, showing a divergence at $h\nu = E_g$. Using the value of E_g thus obtained, we can determine the value of m and hence the nature of transition. Again, from Equation 2, we can get
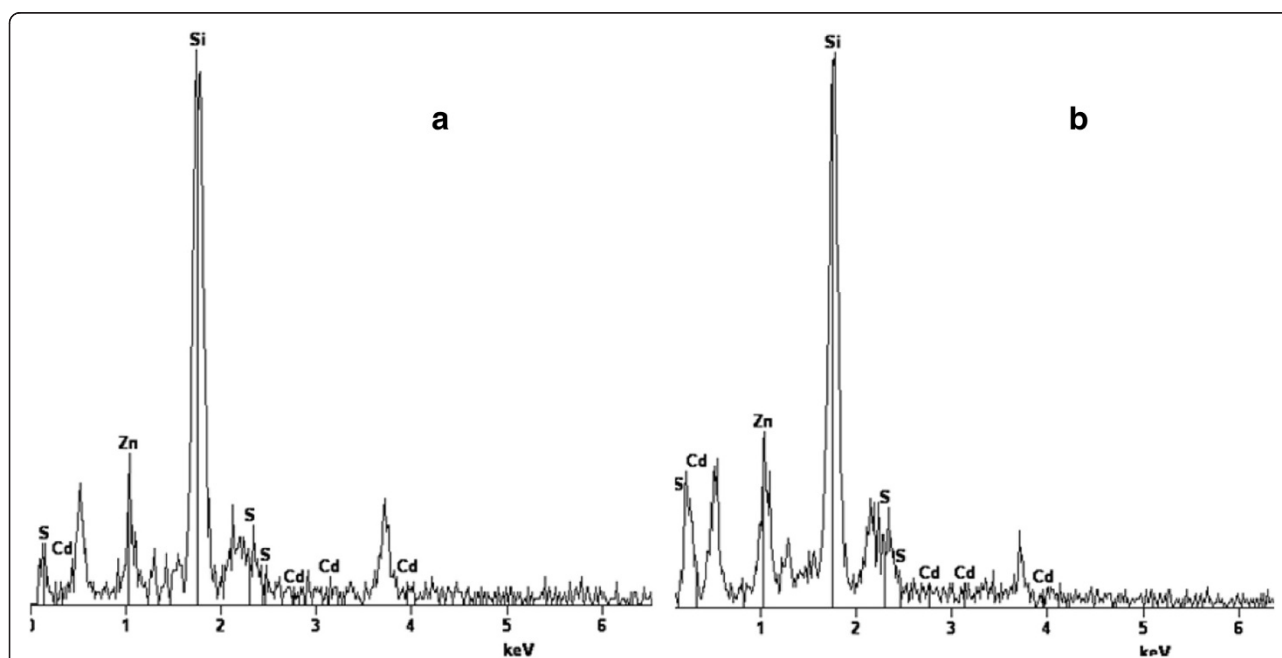
Figure 5 Determination of stoichiometric ratio for $Zn_{1-x}Cd_xS$ QDs. EDAX spectra of $Zn_{1-x}Cd_xS$ QDs produced with Cd content of (**a**) x = 0.04 and (**b**) x = 0.1.

Figure 6 UV-visible absorption spectra of the as prepared $Zn_{1-x}Cd_xS$ QDs dispersed in methanol.

$$\ln(\alpha h\nu) = \ln A + m \ \ln\left(h\nu - E_g\right) \qquad (4)$$

The value of m was determined from the slope of the plot of $\ln(\alpha h\nu)$ versus $\ln(h\nu - E_g)$. The slope in Figure 7b gives the value of m. Using this method, we calculated the value of m for $Zn_{0.9}Cd_{0.1}S$ QDs (0.48) which is comparable to that for direct allowed transition in the bulk material ($m = 0.5$). For all the prepared samples, the values of m are found to be close to the value for the bulk. Now the value of the bandgap can be estimated from the plot of $(\alpha h\nu)^2$ versus $h\nu$, as shown in Figure 8. By extrapolating the straight portion of the graph on the $h\nu$ axis at $\alpha = 0$, the optical bandgaps are calculated, and the values are summarized in Table 1. The obtained bandgap energy is higher than that of the bulk material. Moreover, the bandgap energy decreases with the increase of Cd content in the ZnS QDs [10,12]. This supports the TEM results that the increases of Cd content

result in the increases of the QD size. The optical bandgap of QDs is a combination of the quantum confinement effect arising due to the confinement of the charge carriers and the differences between excitonic energy levels. The quantum confinement resulted to a blue shift of the absorption edge; on the other hand, the excitonic energy caused the red shift of the absorption edge. The observed high values of the optical bandgap energy and its blueshifts with Cd content confirm the formation of $Zn_{1-x}Cd_xS$ QDs. The bulk bandgap energy for different Cd compositions can be obtained from the empirical relation [13,14] given by

$$E_g(x) = E_g(ZnS) + \left[E_g(CdS) - E_g(ZnS) - 0.61\right]x + 0.61x^2 \qquad (5)$$

The incorporation of Cd^{2+} into the ZnS lattice site increases the excitonic energy of the $Zn_{1-x}Cd_xS$ QDs, and as a result, a red shift of the absorption edge is observed. According to the theory for the quantum size effect, the lowest exciton energy in a spherical nanoparticle with a radius R is approximately given by [14]

$$E = E_g + \frac{h^2}{8\mu R^2} - 1.8\frac{e^2}{\varepsilon R} \qquad (6)$$

where E_g, μ, and ε are the bandgap, reduced mass, and dielectric constant, respectively. Since the values of E_g, μ, and ε depend on x in alloy semiconductors, Equation 6 can be modified as follows:

$$E = E_g(x) + \frac{h^2}{8\mu(x)R^2} - 1.8\frac{e^2}{\varepsilon(x)R} \qquad (7)$$

The reduced mass can be obtained by estimating the effective mass of the electron and hole. The band-edge effective mass m_e^* of the carrier can be expressed as [12]
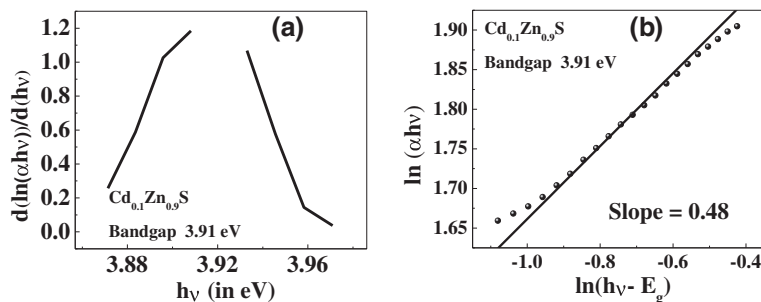
Figure 7 Determination of the bandgap and the nature of transition for $Cd_{0.1}Zn_{0.9}S$ QDs. (**a**) $d(\ln(\alpha h\nu))/d(h\nu)$ versus $h\nu$ curve showing a divergence at $E_g = 3.91$ eV and (**b**) $\ln(\alpha h\nu)$ versus $\ln(h\nu - E_g)$ curve.
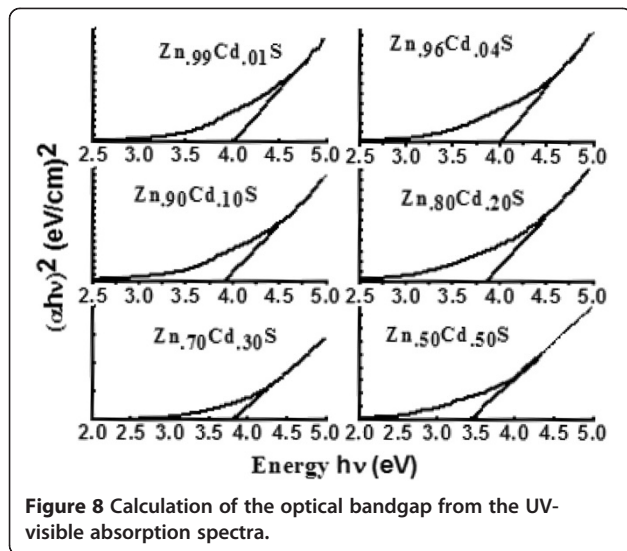
Figure 8 Calculation of the optical bandgap from the UV-visible absorption spectra.

$$\frac{m}{m_e{}^*} = \frac{1}{m^*} = 1 + \frac{P^2}{2mE_g} \qquad (8)$$

So the bandgap E_g can be expressed as

$$E_g = \frac{P^2}{2m}\left(\frac{m^*}{1-m^*}\right) = \frac{P^2}{2m}f(m^*) \qquad (9)$$

where $m^* = \frac{m_e{}^*}{m}$, with m being the mass of the free electron, and P is the momentum matrix element which can be expressed as $P = G$, where G is the smallest

reciprocal lattice vector. Therefore, P becomes equal to $\frac{h}{a}$, where a is the lattice constant, and

$$f(m^*) = \frac{m^*}{1-m^*} \qquad (10)$$

Using Equation 9 in Equation 5, we obtain

$$f(m^*, x) = f(m^*{}_1) + [f(m^*{}_2) - f(m^*{}_2) - b] + bx^2, \qquad (11)$$

where $b = \frac{.61}{P^2/2m}$ and m^*_1 and m^*_2 correspond to the effective masses of the carriers of constituent semiconductors. For the $Zn_{1-x}Cd_xS$ crystal, the b value was found to be 0.06:

$$f(m^*, x) = f(m^*{}_1) + [f(m^*{}_2) - f(m^*{}_2) - 0.61]x \\ + 0.61x^2. \qquad (12)$$

Therefore, by estimating the effective mass of the different values of x, we can calculate the average particle size for the different compositions of semiconductor (using Equation 6). The calculated particle sizes for $Zn_{1-x}Cd_xS$ QDs are summarized in Table 1. The value of the dielectric constant for ZnS is 5.4, and for CdS, it is 5.3. Since there is no appreciable difference between the dielectric constant values of ZnS and CdS, for the calculation of particle size, we have taken $\varepsilon(x) = 5.4$ for all samples. The calculated values of the size of the QDs are well agreed with the value obtained from the X-ray diffraction and TEM analysis.

The room-temperature PL spectra of the $Zn_{1-x}Cd_xS$ QDs are shown in Figure 9. The PL emission spectrum of the neat ZnS QD shows a highly broadened defect emission band with multiple peaks at 378, 400, 420, 450,
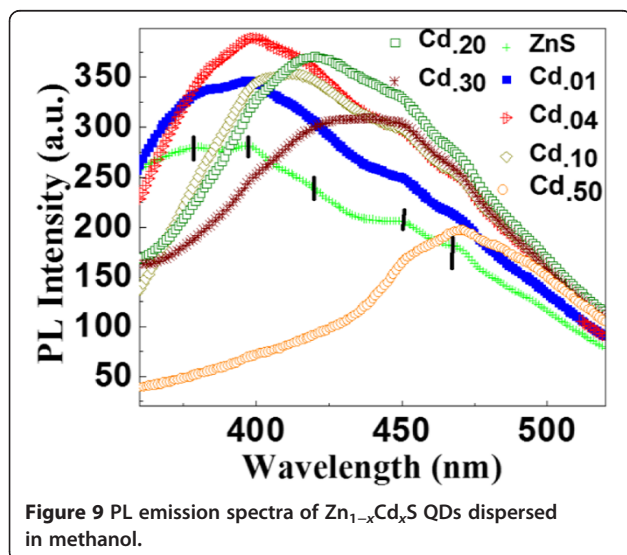
Figure 9 PL emission spectra of $Zn_{1-x}Cd_xS$ QDs dispersed in methanol.
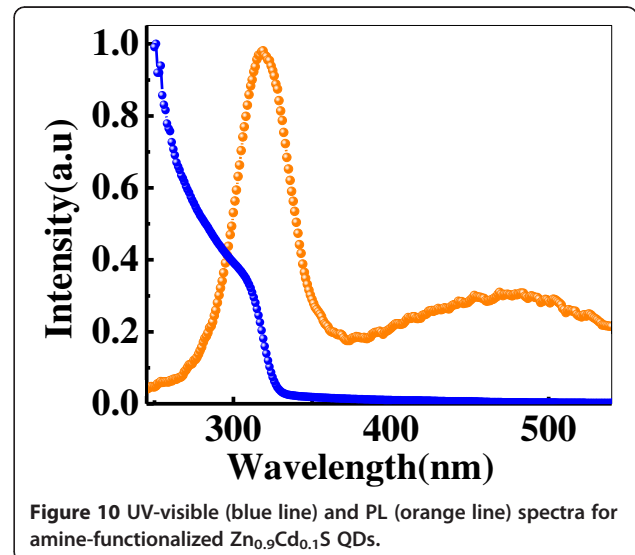
Figure 10 UV-visible (blue line) and PL (orange line) spectra for amine-functionalized $Zn_{0.9}Cd_{0.1}S$ QDs.

and 470 nm. The high-energy side bands (400 and 420 nm) are attributed to the presence of a large concentration of sulfur vacancy centers in the QDs [15,16], whereas the first peak (378 nm) of the emission is attributed to the blue emission from interstitial sites [17]. The fourth and fifth peaks at 450 and 470 nm are related to the blue emission from zinc vacancy and surface defects, respectively. From Figure 9, it can be seen that the peak intensities at 378, 400, and 420 nm for the pure ZnS sample are much smaller than those for the doped samples. It can be explained by the effect of doping. As analyzed above, these peaks are related to native defects. When Cd^{2+} ions are incorporated into ZnS QDs, more defect states are introduced. Therefore, it is reasonable that these defect-related peak intensities are enhanced for the $Zn_{1-x}Cd_xS$ samples compared with the pure ZnS sample. Above 30% doping, the PL peak at 470 nm, due to the lattice defect, dominates all other peaks, although the overall PL intensity decreased at the Cd concentration of 30%. This is due to increase of the surface defect state in $Zn_{1-x}Cd_xS$ crystals. As the concentration of Cd^{2+} increased, it is observed that there is a slight shift in peak position. This shift is due to the increase of particle size and also supports the formation of a $Zn_{1-x}Cd_xS$ nanocrystalline solid solution. All these defect-related emissions can be controlled by functionalizing the prepared QDs with long-chain amine. As-prepared $Zn_{0.9}Cd_{0.1}S$ QDs (100 mg) were mixed with a mixture of 8 ml 1,2-dichlorobenzene and 5 ml oleylamine at room temperature. Under N_2 ambience, the mixture solution was continuously stirred at 150°C for 2 h. After the reaction, the sample was collected by centrifugation at 7,000 rpm for 4 min and washed several times with the acetone and hexane mixture. Figure 10 shows the UV-visible and PL spectra of the amine-functionalized $Zn_{0.9}Cd_{0.1}S$ QDs. The amine ligands (σ-donor) take the position of the vacancies and control the symmetry of the surface closer to that of the core. This phenomenon assists in the compression of the surface defects on the nanoparticle surface by repairing the broken and dangling bonds [18]. This defect-controlled $Zn_{1-x}Cd_xS$ nanocrystalline solid solution can have a wide range of applications including UV light-emitting diodes, efficient phosphors in flat-panel displays, photovoltaic devices, etc.

Conclusion

$Zn_{1-x}Cd_xS$ QDs with different compositions ($0 < x < 0.5$) are successfully synthesized by simple beaker chemistry without using any capping agent or surfactant. X-ray diffraction study confirmed the proper cubic phase formation. Due to the increase of Cd content, all the XRD peaks shifted towards lower diffraction angles. The lattice constant also gradually increased with the Cd content. The XRD results and TEM images showed that

uniform spherical particles were formed and particle sizes varied from 4 to 7 nm as the Cd content was increased from 0 to 0.5. Optical study revealed that the strong absorption edge shifted towards the higher wavelength region; hence, the optical bandgap of the materials decreased with the increase of Cd content. Due to the quantum confinement effect of QDs, the optical bandgap energy is higher than the corresponding value of the bulk material. The PL spectra of the samples are broad and asymmetric and contain five blue emission peaks related to native defects of ZnS.

References
1. Tomihira, K, Kim, D, Nakayma, M: Optical properties of ZnS–CdS alloy quantum dots prepared by a colloidal method. J. Luminescence **112**, 131 (2005)
2. Sarkar, R, Tiwary, CS, Kumbhakar, P, Basu, S, Mitra, AK: Yellow-orange light emission from Mn^{2+}-doped ZnS nanoparticles. Physica E **40**, 3115 (2008)
3. Wang, L, Jiany, Y, Wang, C, Wang, W, Cao, B, Niu, M, Qian, Y: Composition-controllable synthesis and optical properties of non-integral stoichiometry compound $Zn_xCd_{1dx}S$ nanorods. J. Alloys Compd. **545**, 255 (2008)
4. Peny, ZA, Ping, X: Formation of high-quality CdTe, CdSe, and CdS nanocrystals using CdO as precursor. J. Am. Chem. Soc. **123**, 183 (2001)
5. Peng, WQ, Cong, GW, Qu, SC, Wang, ZG: Synthesis and photoluminescence of ZnS:Cu nanoparticles. Opt. Mater. **29**, 313 (2006)
6. Arora, S, Manoharan, SS: Structural and photo luminescent properties of uncapped nanocrystalline $Cd_{1-x}Zn_xS$ solid solutions. Opt. Mater. **31**, 176 (2008)
7. Leverenz, HW: An Introduction to Luminescence of Solids. Wiley, New York (1950)
8. Zu, S, Wang, Z, Liu, B, Fan, X, Qian, G: Synthesis of nano-$Cd_xZn_{1-x}S$ by precipitate-hydrothermal method and its photocatalytic activities. J. Alloys Compd. **476**, 689 (2009)
9. Tiwary, CS, Kumbhakar, P, Mitra, AK, Chattopadhyay, K: Synthesis of wurtzite-phase ZnS nanocrystal and its optical properties. J. Lumin. **129**, 1366 (2009)
10. Jana, S, Maity, R, Das, S, Mitra, MK, Chattopadhyay, KK: Synthesis, structural and optical characterization of nanocrystalline ternary $Cd_{1-x}Zn_xS$ thin films by chemical process. Physica E **39**, 109 (2007)
11. Furdyan, JK: Diluted magnetic semiconductors. J. Appl. Phys. **64**, R29 (1988)
12. Kulkarni, SK, Winkler, U, Deshmukh, N, Borse, PH, Fink, R, Umbach, E: Investigations on chemically capped CdS, ZnS and ZnCdS nanoparticles. Appl. Surface Science **169**, 438 (2001)
13. Ammar, AH: Structural and optical properties of $Zn_xCd_{1-x}Se$ thin films. Physica B **296**, 312 (2001)
14. Ray, SC, Karanjai, MK, DasGupta, D: Deposition and characterization of $Zn_xCd_{1-x}S$ thin films prepared by the dip technique. Thin Solid Films **322**, 117 (1998)
15. Manzoor, K, Aditya, V, Vadera, SR, Kumar, N, Kutty, TRN: Enhanced electroluminescence properties of doped ZnS nanorods formed by the self-assembly of colloidal nanocrystals. Solid State Communications **135**, 16 (2005)
16. Rao, CNR, Müller, A, Cheetham, AK (eds.): The Chemistry of Nanomaterials: Synthesis, Properties and Applications, p. 380. Wiley, Weinheim (2007)

17. Arora, S, Manoharan, SS: Large shift in the photoluminescent properties of Mn^{2+}-doped nanosized CdS–ZnS solid solutions. J. Solid State Chem. **144**, 319 (2007)
18. Mohapatra, J, Mitra, A, Bahadur, D, Aslam, M: Surface controlled synthesis of MFe_2O_4 (M = Mn, Fe, Co, Ni and Zn) nanoparticles and their magnetic characteristics. CrystEngComm **15**, 524–532 (2013)